Hindawi
Adsorption Science & Technology
Volume 2022, Article ID 8684737, 13 pages
https://doi.org/10.1155/2022/8684737

Research Article

Hydrothermal Carbonization of Waste Sugarcane Bagasse for the Effective Removal of Emerging Contaminants from Aqueous Solution

G. Prasannamedha [1,2] **and P. Senthil Kumar** [1,2]

[1]*Department of Chemical Engineering, Sri Sivasubramaniya Nadar College of Engineering, Kalavakkam, Chennai 603110, India*
[2]*Centre of Excellence in Water Research (CEWAR), Sri Sivasubramaniya Nadar College of Engineering, Kalavakkam, Chennai 603110, India*

Correspondence should be addressed to P. Senthil Kumar; senthilkumarp@ssn.edu.in

Received 22 October 2021; Revised 11 December 2021; Accepted 16 December 2021; Published 6 January 2022

Academic Editor: George Kyzas

Porous carbon spheres were fabricated from sugarcane bagasse using a sustainable hydrothermal carbonization process followed by alkali impregnation inert atmosphere activation. Developed spheres were technically analysed for their chemical science, structural morphology, texture, porosity with respect to size distribution, and thermal degradation. Spheres are functionally enriched with oxygenated groups showing amorphous nature portraying as a smooth surface. After activation, intensity of functional groups is reduced due to reduction reaction by KOH thereby yielding highly rich porous carbon. The active surface area developed on spheres is 111 m^2 g^{-1} holding pores that are mesoporous in nature. Resistance to thermal exposure using TGA showed that decomposition of hemicelluloses followed by cellulose yielded aromatized carbon-rich skeleton through thermal degradation of carboxyl and hydroxyl groups. Developed carbon was found to be effective in removing Ciprofloxacin Hydrochloride from water with maximum adsorption capacity of 110.008 mg g^{-1}. Mechanistic removal followed pseudo-second-order kinetics along with Freundlich mode of adsorption. The presence of carboxylic and hydroxyl groups in porous carbon favoured elimination of CPF from water. The development of HTC-derived carbon helped conserving the energy thereby reducing the cost requirement.

1. Introduction

Generation of carbon spheres (CS) had attracted everyone's side in the field of research as they find numerous applications as adsorbents, support for catalysts, energy conversion, and energy storage in lithium batteries. There are multiple ways available for preparation of CS, namely, chemical vapour deposition, pyrolysis of organic compound, polymerization, arc discharge, plasma process, and solvothermal. All the above method has their own pros and cons. Additionally, these methods use chemicals as agents for preparation of CS along with some reducing agents or catalysts if needed [1]. Among them, solvothermal (HTC) synthesis is focussed more due to its versatility, easy mode of application. It involves hydrothermal carbonization (HTC) which is accompanied by thermal conversion of wet biomass at moderate temperature and autogenous pressure. HTC is influenced by certain parameters like carbonization temperature, residence time, substrate concentration, heating rate, pressure, and reaction pH [2, 3]. The major ingredient in the production of CS using HTC is waste biomasses that are mainly coming from agriculture, forest, industrial waste that are rich in cellulose, starch, pectin like rice husk, cotton fibres, wheat straw, sugarcane bagasse, orange peel, and paper and pulp. This process is highly reliable as it involves heating aqueous solution of biomass which is simple, eco-friendly and inexpensive [4]. Solid product obtained in HTC which is considered to be CS is homogenous and hydrophobic in nature. One of the main advantages of HTC process is it is operated under saturated steam pressure

that avoids evaporation energy thereby reducing the energy for heating the biomass which is considered comparatively less than active drying [5]. It could be understood that HTC is performed in the temperature range of 180-350°C, operated in the pressure range of 2 to 6 MPa for about 5 to 240 minutes [6].

Material fabricated from HTC is a carbonaceous product having uniform chemical and structural property. The structure of carbon is in the form of sphere having hydrophobic functional groups on its core shell whereas hydrophilic compounds in the outer ring [7]. CS evolving from HTC has no pores unless they are synthesised in the presence of template or subjected to activation methods [8]. As reported by [9], these spheres low very less surface area thereby portraying less pores on their surface that are not sufficient to be used for environmental cleaning and other applications. Hence, they were activated at various atmospheres for improving their surface area and active pores that are responsible for holding pollutants.

Activation of spherical carbon is achieved by inert gas activation using alkali impregnation, steam, hydrogen peroxide and phosphoric acid activation, and microwave assistance activation. Upon activating carbon spheres, they were found to have more advantages compared to normal powdered activated carbon like high mechanical strength, high wear resistance, low ash content, appreciable adsorption capacity, high micropore volume with controlled size distribution, and high bulk density having smoothly appearance [10]. From previous studies, it could be understood that upon activating, using hydrogen peroxide in microwave assistance yields porous carbon with 1274 $m^2\ g^{-1}$ [11], whereas activating carbon spheres using phosphoric acid in the form of precursor induced excellent surface area in the range of 1309 to 1897 $m^2\ g^{-1}$ [12, 13]. Alkali impregnation followed by inert gas activation at high temperature produced activated carbon spheres with good porosity and active surface area around 1200 $m^2\ g^{-1}$. The main mechanism of formation of pores with improved surface area is due to reduction reaction carried out by NaOH/KOH on the surface of carbon skeleton [14]. The effect of various modes of activation in favouring surface area might reduce the intensity of oxygenated functional groups on carbon skeleton which is as follows $CO_2 < H_3PO_4 < KOH < NaOH$ [15].

Normally, the HTC process helps in conserving energy as the process of pretreatment of biomass is less. The use of raw agricultural waste can reduce affecting the surrounding environment because one of the most common human activities is burning of farming residues like bagasse, wheat straw, barley waste, rice husk, and paddy which may increase the concentration level of air pollutants that are most commonly monitored by the public sector. An increase in these pollutants might induce respiratory diseases in human beings. Hence, recycling of these crop wastes is encouraged in eradicating environmental contamination [16]. This research is focussed in fabrication of CS and ACS from sugarcane bagasse using normal Teflon lined stainless steel autoclave and to study its structural morphology, texture, chemical groups, and porosity for defining its predetermined structure which could be employed in removing emerging contaminant (Ciprofloxacin Hydrochloride) from water. Batch adsorption studies were performed at optimum condition for defining adsorption influencing parameters like pH, adsorbent dosage, and concentration of pollutant for identifying the adsorption kinetics and mechanistic removal between adsorbent and adsorbate.

2. Experiments

2.1. Materials and Methods. All chemicals used in the experiments are of analytical grade. Bagasse waste residue was procured from nearby small scale juice plant at Chennai. Stainless steel autoclave lined by Teflon material was designed and manufactured by M/s. Fazal Engineering, Chennai, India. Ciprofloxacin Hydrochloride tablets were collected from Apollo Pharmacy for assessment.

2.2. Synthesis of Spherical Carbon. Sugarcane bagasse was crushed, chopped into fine powder using a mixer. The fine powder was sieved using mesh of size 160 μm in diameter in order to split small fibres from super fine powder. This powder was soaked in 0.1 M NaOH solution at 80°C for 4 hours for removing inorganic minerals followed by washing thoroughly with water. Nearly 3 to 4 g of dried bagasse was sealed airtight by adjusting screws and nuts of Teflon lined stainless steel high-pressure autoclave and heated at 190°C for 14 hours. As soon as the reaction was completed, the reactor was cooled down and a brownish-black semisolid mixer was collected. This solid compound was washed continuously using acetone, ethanol, and distilled water until the reddish-brown colour filtrate turns into colourless filtrate. Finally, solids were vacuum dried at 70–80°C for overnight which is carbon spheres (CS).

2.3. Preparation of Activated Spherical Carbon. CS was activated using the KOH impregnation method in which prepared CS and KOH were mixed in 1 : 2 ratio and normally stirred rate nearly 4–6 hours and at hot air oven. This dried product was powdered and placed under nitrogen atmosphere at 700°C for two hours at 3°C/min. The flow rate of nitrogen is maintained at 10 mL/min. As soon as the reaction stops, the product was removed and washed completely using 0.1 mol/L HCl until the product turned neutral. Finally, obtained solid product was air dried and named as activated carbon spheres (ACS-K).

2.4. Characterization. Both CS and ACS were characterized for their functional group, surface morphology, surface area and porosity, size of the particle, and its response at varying temperatures. Surface morphology and microshaped structure were studied using a scanning electron microscope (SEM) made from Hitachi, Japan, along with an EDAX analyser. The presence of functional groups was studied using Fourier Transform Infrared (FTIR) Spectroscopy in Spectrum Two FT-IR/Sp 10 software, Perkin Elmer, USA. Amorphous nature of CS and ACS was studied in X-Ray Diffraction (XRD) using PXRD, PANalytical X'Pert Pro-Diffractometer using monochromatic Cu$K\alpha$ radiations. The presence of pore and surface area was studied using

Quantachrome pore size and surface area analyser at normal conditions. The size of the particle distributed in the sample was analysed using HORIBA Laser Scattering Analyser, LA-960. Nature of degradation of polymers that are present in bagasse with respect to weight loss at varying temperature was studied using Thermogravimetric Analyzer–Differential Scanning Calorimeter (TGA-DSC), Perkin Elmer STA 600. Zeta potential for ACS-K was studied using Horiba Scientific SZ-100 which was used for analysing zero point charge in defining adsorbate and adsorbent interaction with respect to pH.

2.5. Batch Adsorption Studies. Batch adsorption experiments were performed using ACS-K in 100 mL of Ciprofloxacin (CPF) solution at standard room atmosphere. After the completion of adsorption, the filtrate was filtered through 0.22 μm nylon membrane and estimated for quantification of CPF using a UV-Visible spectrophotometer (LARK Li-UV-7000) at a wavelength of 275 nm. Standard protocol was followed for defining the adsorption influencing parameters like pH, dosage, and pollutant concentration. Effect of contact time was studied using three different kinetic equations whereas mode of interaction of adsorbent and adsorbate was analysed using three isotherm models. The nonlinear mathematical equations used for estimation of all adsorption kinetics and isotherm parameters are given in Table S1. Regeneration studies for adsorbent were carried for estimating its capacity which is discussed in the later sections.

3. Results and Discussion

3.1. Elemental Examination. Element composition of CS and ACS-K was taken for gaining knowledge about the presence of C, N, H, and O. Table S2 provides the detailed description about elements found in CS and ACS-K. It could be noticed that carbon content of CS increased up to 62.37% which shows that carbonization occurs at 190°C whereas after activation, ACS-K show 73.83% of carbon portraying that inert activation improved carbonization thereby exposing the amorphous nature of carbon. The content of oxygen was estimated by subtracting relative C, N, and H fractions that showed an opposite behaviour to elemental carbon [17, 18]. Additionally, it could be observed that reduced O/C and H/C values indirectly provide evidence for dehydration and decarboxylation reactions that could be dominating during the HTC process in yielding CS, thereby resulting in high aromaticity [19]. The yield was calculated based on the following equation [20]:

$$\text{Yield}\,(\%) = \left(\frac{\text{HTC product weight}}{\text{Raw biomass weight}}\right)100. \quad (1)$$

3.2. XRD Analysis. XRD profile is used for understanding the amorphous/crystalline nature of fabricated material. CS and ACS-K were analysed in XRD whose profiles are given in Figures 1(a) and 1(b). XRD pattern for CS shows a one broad hump in the range of $2\theta = 20.6$°C that denotes the amorphous nature of carbon. These broad peaks of CS are assigned to (002) and (101) planes of material fabricated from HTC [21]. After activation using KOH in an inert atmosphere at high temperature, a slight derivation had been witnessed in the XRD profile. Two broad humps at $2\theta = 21.2^\circ$ and 43.1° could be seen indicating the amorphous nature of carbon [22]. Background pointer between 10° and 20° might be because of availability of micropores in carbon with turbostratic graphitic structure [23]. The peak around 40°–44° for ACS-K indicates that degree of activated carbon is increased during activation at high temperature. This shows that the structure of carbon is disordered in nature filled with graphite layer thereby favouring the movement of electrons during pollutant interactions [5, 24].

3.3. SEM/EDAX Analysis. SEM analysis identifies the structural morphology of material fabricated using HTC from sugarcane bagasse shown in Figures 2(a) and 2(b). After HTC treatment, a huge number of smooth surfaced spherical carbon were generated in an agglomeration state that is shown in Figure 2(a) [25–27]. This could be due to accumulation of certain polymers having polyaromatic structures that are commonly identified in raw material (bagasse) during chemical reactions [28]. The absence of pores on the surface portrays CS to be smooth which could be due to wet reaction in the compressed water within the closed reactor. This was further confirmed in BET analysis which is discussed in the coming section [25, 26, 29]. ACS shows slight variation in the form of formation of pores and cavities on the carbon surface. This is due to activation using KOH at high temperature in an inert atmosphere. These pores are formed due to release of CO_2 and CO that are obtained as by-product in the chemical reaction of carbon with alkalis. These activating agents are responsible for narrowing the distance between aromatic layers of carbon material thereby leading to destruction of carbon surface through intercalation of KOH [30]. Additionally, interaction of carbon with alkali favours enhancement in surface area for effective adsorption. From Figure 2(b), it could be seen that after activation, spheres of size 1 to 5 μm are destructed in their structure thereby forming a complete size in the range of 195 nm to 298 nm. EDAX for CS and ACS-K are shown in Table S3. For CS, the spectrum shows huge quantity of carbon and oxygen atoms. Carbon serves as a skeleton in holding the oxygenated function groups on its surface. The presence of carboxylic, hydroxyl, and carbonyl groups are confirmed in the FTIR spectrum. After activating CS using KOH yielded carbonaceous structure followed by reduction in amount of oxygenated functional groups. This is due to intimate oxidation and reduction induced by an activating agent.

3.4. BET Analysis. As described in Table S4, BET analysis provides details about the active surface area, nature of pore formed and distributed on the active and nonactive surface of the carbon formed from sugarcane bagasse using HTC which is shown in Figure 3. It could be witnessed that CS showed very less active surface area with superior mesopores on its surface. The similar observation was made in the synthesis of carbon spheres from glucose using HTC [31]. The adsorption capacity of CS is comparatively very low than ACS as active surface area is less. Pores are one major

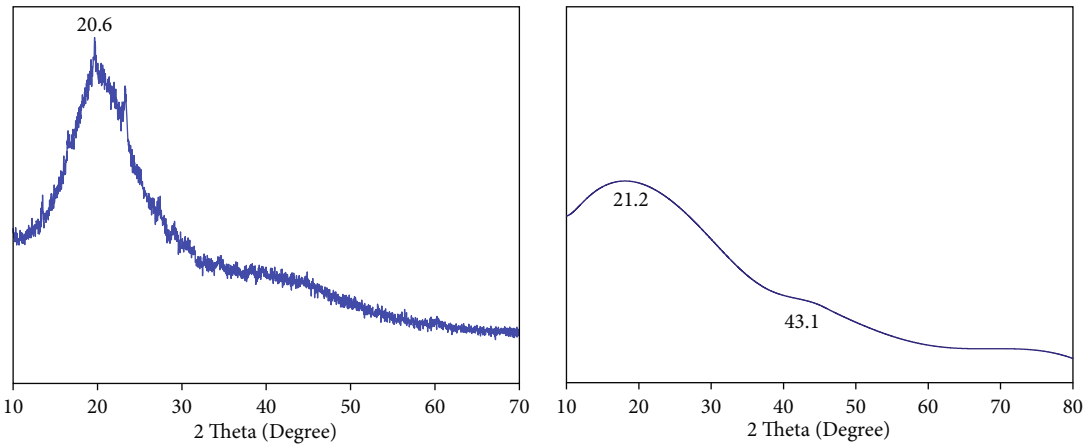

(a) XRD profile of CS (b) XRD profile of ACS activated using KOH

Figure 1: (a, b) XRD profile of CS and ACS.

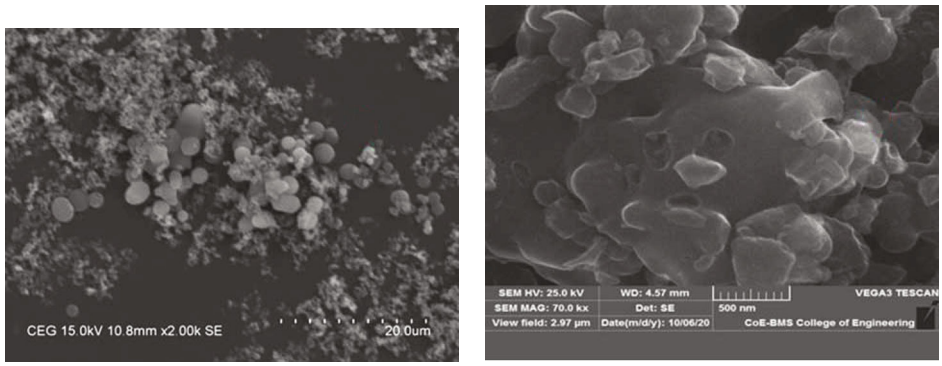

(a) (b)

Figure 2: (a, b) SEM analysis projecting morphology of CS and ACS.

holding hand for incoming pollutants to be trapped on the surface of the adsorbents. After activation using KOH showed a sharp rise in BET surface area thereby developing numerous pores showing active area of 111 m^2 g^{-1}. The average size of pore was noticed as 3.470 nm (2–50 nm) is related to mesopore denoting that material is filled with mesoporous structure. The hysteresis loop of adsorption-desorption isotherm of CS showed an isotherm with low pores on its surface portraying limited surface area [32], whereas upon activating CS, using KOH impregnation method showed combined type II and IV isotherm indicating the presence of mesopores on its structure [28, 30]. Pore size distribution is significant in defining the structural morphology of synthesised material through which kinetic and equilibrium properties of the material could be identified [33]. The pore sizes that are distributed on CS and ACS are shown within BET analysis diagram. From the results, it could be seen that CS lacks proper development of pores on its surface whereas after activating it with KOH at high temperature in an inert atmosphere, mesoporous structure was witnessed.

3.5. Particle Size Distribution. To understand the effect of activation at high temperature in an inert atmosphere using alkali on HTC-derived CS, particle size distribution investigated is shown in Figure S1. For CS, the size of particle was measured in terms of 0.1 to 1000 μm whereas for ACS-KOH, it is reduced to 10 to 10000 nm. For ACS-K, the density of particle distribution shows trimodal distribution with the first one ranging from 10 nm to 13.615 nm, the second one from 13.615 nm to 100.841 nm, and the third one from 100.841 nm to 8385.525 nm. The maximum particle size of ACS-K was found to be 317.59 nm. For CS, the density of population shows bimodal distribution with the first one from 0.443 μm to 24.546 μm and the second one from 24.546 μm to 188.131 μm. The maximum size of particle was found to be 8.461 μm.

3.6. Thermogravimetric Analysis (TGA). The TGA and DTG curves of CS and ACS-K are shown in Figure S2. TGA curve below 100°C denotes the loss of water molecules from biomass during heat treatment. In HTC-CS, weight loss is shown in between 158°C to 303°C and 303°C to 520°C denoting preservation and decomposition of cellulose and hemicellulose, respectively [34]. Major loss could be observed after 340°C denoting the decomposition of oxygenated functional groups and oxidation of conjugated

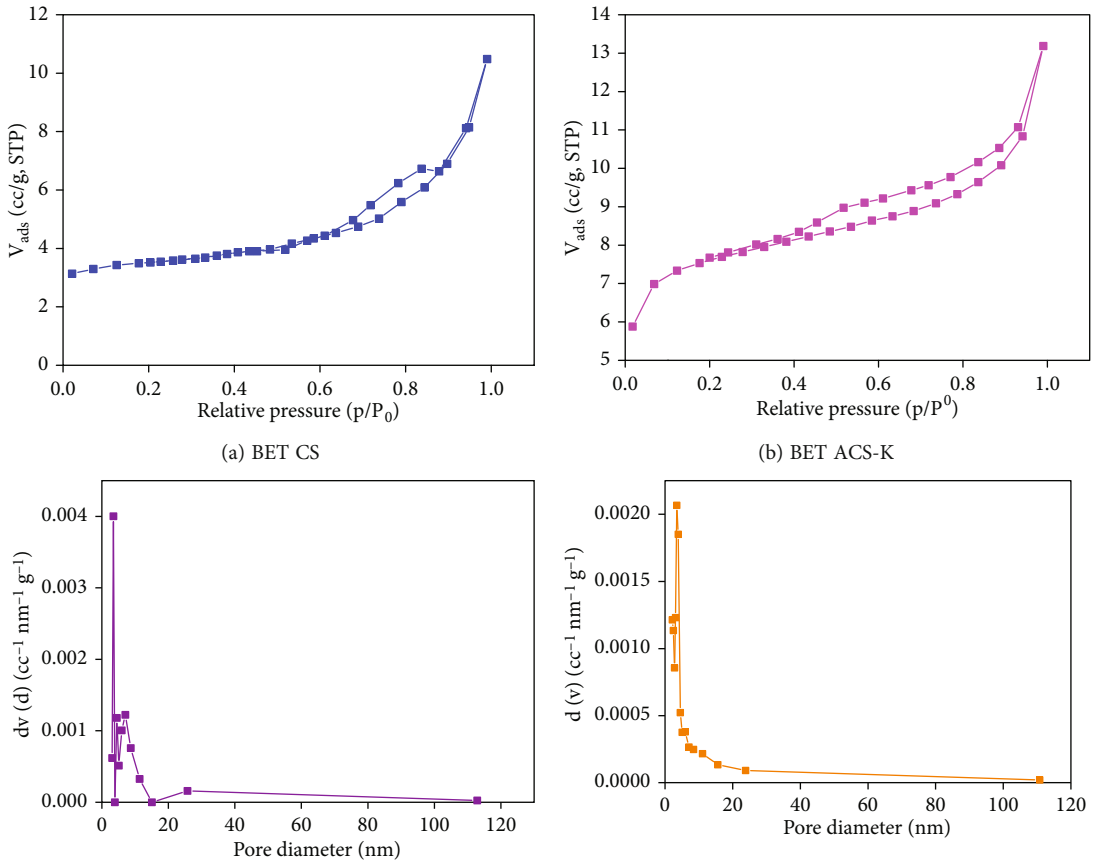

Figure 3: BET analysis of CS and ACS. (a) and (b) show nature of pores on CS. (c) and (d) for ACS/KOH.

carbon skeleton [35]. Similar stages of weight loss could be observed in ACS-K in which below 100°C loss of moisture whereas above 200°C thermal degradation of hydroxyl and carboxyl groups [36]. Stage after 600°C indicates aromatization of structural network in carbon [37]. The DTG curve of HTC CS shows a sharp-edged peak after 500°C which could be assigned to lignin residue of the chosen sample [38].

3.7. FTIR Spectrum Analysis. Spectrum showing functional moieties on the carbon skeleton formed from sugarcane bagasse using HTC before and after activation is shown in Figures 4(a) and 4(b). As an inference, availability of functional groups is higher in CS compared to ACS. Among them, the hydroxyl group (O-H) is more common and found to be available at two peaks, namely, 3430 cm^{-1} and 1028 cm^{-1} (aliphatic C-OH). The peak at 3433 cm^{-1} shows higher intensity of the O-H group thereby suggesting the lower degree of carbonisation process whereas at 1028 cm^{-1}, intensity is very less portraying that stretching of carbon skeleton is higher through dehydration reaction thereby suggesting the higher degree of carbonisation [39]. Two small and adjacent mounts at 1612 cm^{-1} and 1712 cm^{-1} peaks correspond to the presence of C=C and C-OH groups on the carbon skeleton denoting the presence of humins [31, 40]. Additional two tiny bands at 2923 cm^{-1} and 2846 cm^{-1} were identified as availability of the aliphatic C-H group [41]. The most prevalent structure of hydrothermal carbon is aromatization of carbon sequence leading to arrangement of graphitic carbon series as multiple layers [42]. The presence of bands at 866 cm^{-1} is attributed to aromatic C-H due to aromatization reaction [31]. Other spectra showing ketonic, carbonyl, and hydroxyl groups at 1518, 1285, and 1028 cm^{-1}, respectively, are a group of polar functional groups that could be formed due to dehydration, dehydrogenation, and aromatization during carbonisation process [25, 26, 43].

After activation of CS with KOH as shown in Figure 4(b), while comparing the spectrum of CS with ACS-K, it could be seen that the KOH spectrum shows very less amount of intense functional moieties. This could be due to the fact that KOH is a strong reducing agent thereby promoting reduction of oxygenated groups on the carbon structure [10]. One arbitrary observation found in ACS is shift in spectrum, to illustrate after activation primary alcohol peak at 1028 cm^{-1} is negligible in ACS which could be due to the reduction/dehydration reaction between alkali and functional groups on carbon. The shift in peaks at 1128 cm^{-1} corresponds to the C-O group of aromatic esters and carboxylic acid whereas at 1455 cm^{-1} is C-H bending indicating the carbonisation process during activation [31].

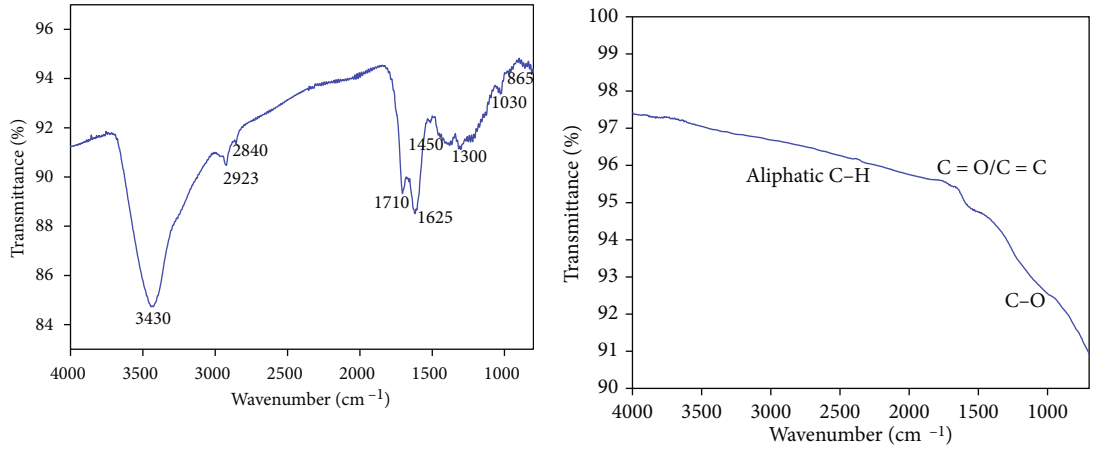

(a) IR spectrum for CS

(b) IR spectrum for ACS-K

FIGURE 4: (a, b) FTIR analysis for CS and ACS-K showing variation in the presence of functional groups.

3.8. Adsorption Results

3.8.1. Factors Influencing Adsorption Process

(1) Impact of Adsorbent Dosage and Pollutant Level. For identifying optimum dosage of adsorbent, ACS-K varied from 0.1 to 1.0 g L^{-1} with initial concentration of CPF as 50 mg L^{-1} at pH 6.3 ± 0.1. It was witnessed that as the adsorbent concentration increases, removal efficiency decreased which could be accumulation of adsorbents thereby reducing the exposure of active sites. It could be seen that maximum removal efficiency of nearly 99.4% was achieved in 0.1 gL^{-1}. As the concentration of CPF amplified from 5 mg L^{-1} to 50 mg L^{-1}, adsorption was found to be lower which could be due to inner collision between CPF units [28]. Figure 5(a) depicts the effect of adsorbent dosage in removing CPF from water, and Figure 5(d) shows the effect of CPF concentration

(2) Consequence of pH. To investigate the influence of solution pH on ACS-K in removing CPF, different pH values were taken ranging from pH 2 to 12. While performing pH experiment, optimum concentration of CPF was maintained at 50 mg L^{-1} and 0.1 gL^{-1} adsorbent dosage at room temperature which was chosen. It could be witnessed that removal efficiency was best in pH of 3 to 8 whereas decreased after pH 8. Maximum elimination was observed at the pH range of 6 to 8 [44]. Figure 5(b) shows the result of solution pH in removing CPF. It is well known that pK_a values of CPF range from 6.1 to 8.7 which denotes that at $pK_{a1} < 6.1$, CPF remains positive whereas in $pK_{a2} < 8.7$, CPF remains negative as shown in species distribution (Figure S3) [45, 46]. CPF is a pharmaceutical organic compound with amphoteric features. At $pK_{a1} < 6.1$, CPF is positive because of availability of the carboxylic acid group whereas at $pK_{a2} < 8.7$, CPF turns negative due to the amine group in the piperazine ring. Decreased removal at pH < 3 is due to electrostatic repulsion between CPF^+ and positively charged surface on ACS-K. Whereas above pH > 8, CPF^- could be in competitive for OH^- for active adsorption sites hence decreased removal of CPF was observed [47]. It could be seen that maximum removal was witnessed near 6.9 from Figure 5(b). With respect to P_{ZPC} of ACS-K (6.2) as shown in Figure 5(c), it could be stated that maximum adsorption at pH 6.4 could be due to electrostatic interaction between CPF and ACS-K as at this pH, CPF remains near positive and ACS-K stays negative [48].

3.8.2. Kinetics Followed by CPF. Adsorption of CPF on ACS-K is well explained by pseudo-first order (PFO) [49], pseudo-second order (PSO) [50], and intraparticle diffusion [51]. The parameters estimated in each model are listed in Table 1. The kinetic model defines the relationship between effective adsorption capacities of adsorbent with respect to equilibrium time. From the results obtained, it could be identified that as the concentration of CPF increases, equilibrium adsorption capacity increased. Additionally, time to attain equilibrium state was longer with respect to higher concentration of CPF which could be justified as adsorption rate constant decreased as shown in Table 1 [52, 53]. From Figures 6(a) and 6(b), it could be witnessed that equilibrium adsorption capacity of ACS-K increased with an increase in concentration of CPF. Results clearly state that the PSO model is best fitted (R^2 -0.99) indicating thereby suggesting that mechanism of adsorption is through chemical mode of interaction [44]. Further Weber-Morris intraparticle diffusion was used to identify the stages of diffusion of CPF within the adsorbent. Figure 6(c) suggests that ACS-K undergo three successive stages in reaching equilibrium: external diffusion, pore diffusion, and sorption process [54]. Hence, it could be stated that chemical means of interaction favours the removal of CPF from water. From FTIR studies, the presence of –OH and –COOH groups on ACS-K might favour the removal process of CPF [47].

3.8.3. Isotherm Model. The isotherm model helps in identifying the interaction of adsorbent with adsorbate. It is used in designing adsorption process by understanding the mechanism of adsorption and homogeneity and heterogeneity of

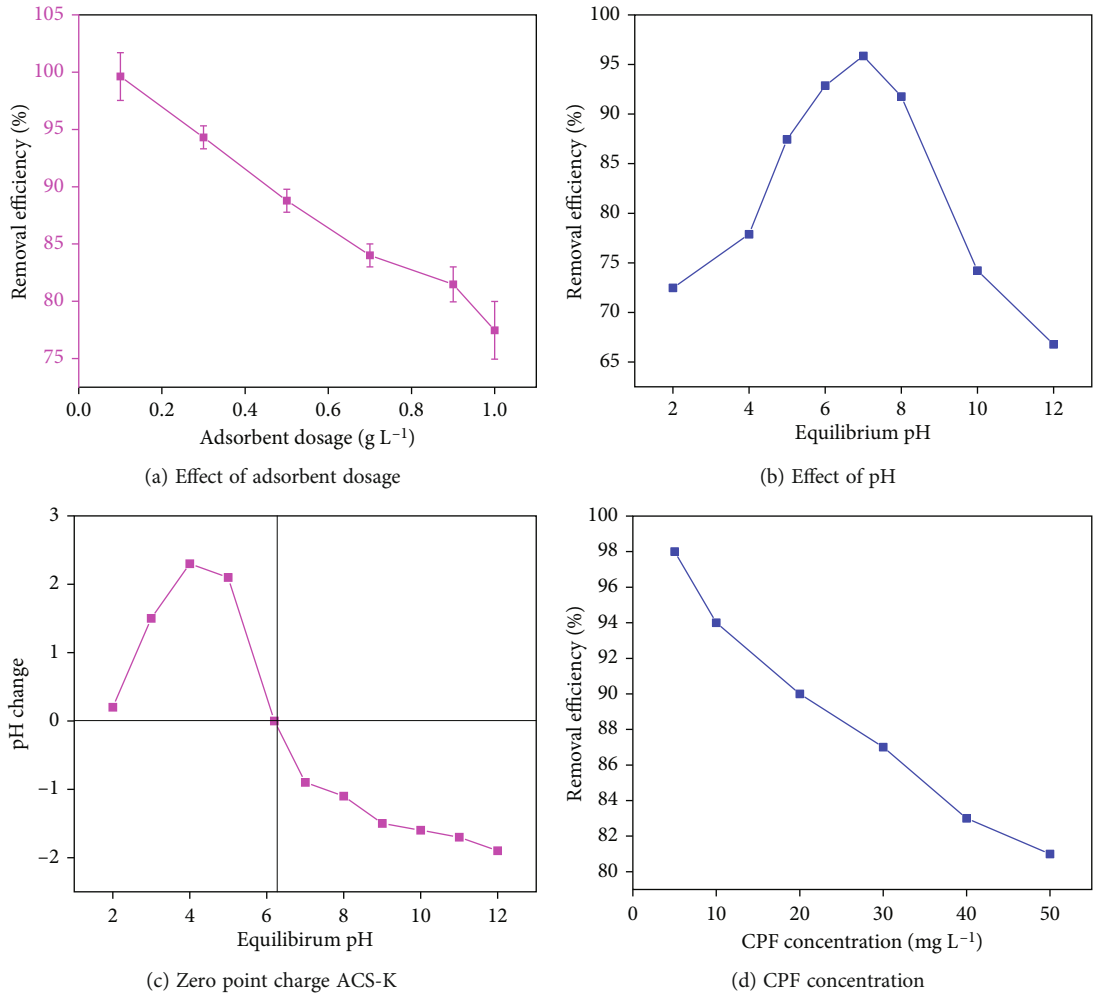

(a) Effect of adsorbent dosage

(b) Effect of pH

(c) Zero point charge ACS-K

(d) CPF concentration

Figure 5: (a, b) Effect of adsorbent dosage and equilibrium pH in removing CPF from water, (c) zero point charge of ACS-K, and (d) effect of CPF concentration with respect to removal.

Table 1: Parameters estimated in adsorption kinetics in removing CPF.

C_o (mg/L)	q_e (exp) (mg/g)	Pseudo-first order				Pseudo-second order				Intraparticle diffusion				
		k_1 (min^{-1})	q_e (cal) (mg/g)	R^2	Δq (%)	k_2 (g/mg·min)	q_e (cal) (mg/g)	h (mg/g min)	R^2	Δq (%)	k_p (mg/g·min$^{(1/2)}$)	C	R^2	Δq (%)
30	72.568	0.0729	66.971	0.969	2.453	0.0017	72.604	8.961	0.978	0.114	2.152	50.124	0.978	1.265
50	93.656	0.065	84.41	0.835	5.071	0.0011	93.017	9.517	0.983	0.015	3.422	54.76	0.984	1.529

adsorbent surface. In this research, mode of contact of CPF with ACS is well explained by Langmuir [55], Freundlich [56], and Temkin and Pyzhev [57] models. Table 2 projects the parameters estimated in isotherm models that plainly shows that the Freundlich model best suits the adsorption process with greater R^2 and lesser Δq_e values. This shows that adsorption mechanism is heterogeneous and multilayer process. The determined monolayer adsorption capacity of ACS with CPF was estimated to be 110.008 mg g^{-1} [58]. While comparing with earlier examination, the obtained capacity is quite less which could be due to accumulation of carbon particles one thereby promoting limited exposure of active sites which is confirmed SEM analysis [3]. In addition, process is considered as favourable and cooperative adsorption if the value of $1/n < 1$ and $1/n > 1$, respectively. The value of $1/n$ is less than 1 thereby CPF is favourably adsorbed by ACS [59]. In addition, the value of exponent $n > 1$ showing adsorption process is physical, simple, and fast [44]. In the Temkin model, the value of b_T is less than 80 kJ/mol, indicating the physical mode of interaction [45]. Hence, it could be concluded that mechanistic removal of CPF from water by ACS is through monolayer mode of communication with appreciable adsorption capacity. Figure 6(d) shows the adsorption capacities of CPF with ACS. While comparing activated carbon that is not evolved from hydrothermal carbonisation as shown in Table 3, HTC carbons are

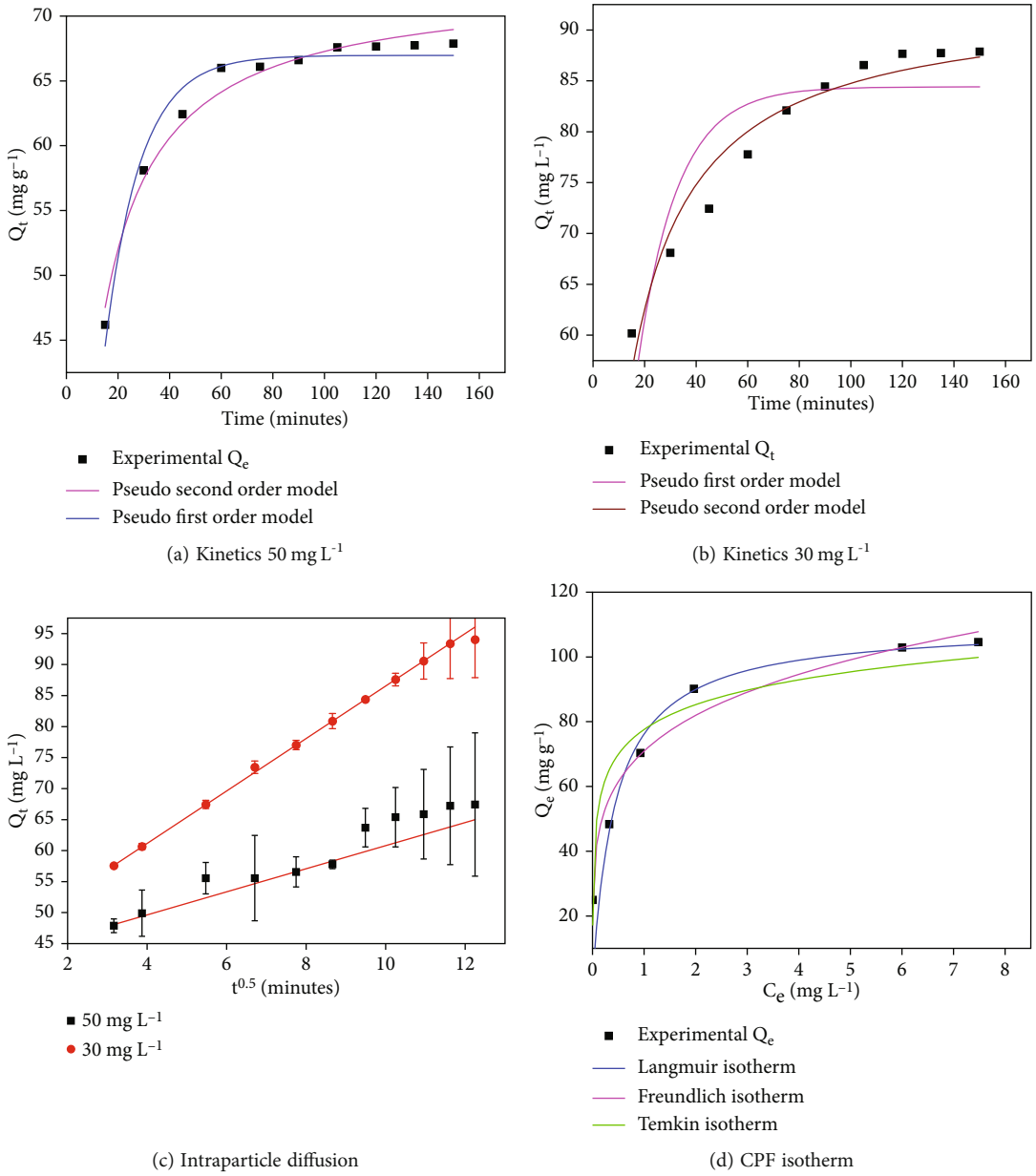

Figure 6: (a, b) Kinetics followed by CPF adsorbed by ACS, (c) pore diffusion effect of CPF in ACS, and (d) CPF isotherm.

Table 2: Adsorption isotherm pertaining to CPF interaction with ACS.

Adsorbent	Isotherm model	Isotherm name	Parameters	R^2	Δq_e (%)
ACS	Two parameter isotherm models	Langmuir isotherm	$q_m = 110.008$ mg/g $K_L = 2.2446$ L/mg	0.887	0.308
		Freundlich model	$n = 4.8117$ $K_F = 7.9349$ (mg/g) (L/mg)$^{1/n}$	0.971	0.905
		Temkin	$B = 23.035$ $b_T = 109.371$ J/mol $A = 25.274$ L/g	0.911	4.252

Table 3: Comparison on the performance of ACS-K with other adsorbents in removing ciprofloxacin.

Precursor	Activation method	Isotherm model	Adsorption capacity (mg g^{-1})	Reference
Prosopis juliflora wood	Acid activation	Langmuir model	250	[48]
Desilicated rice husk	Physical activation using steam as activating agent	Langmuir model	461.9	[67]
Graphene and granular activated carbon	—	Langmuir model	323	[68]
Fruits of Jeriva	Chemical activation using $ZnCl_2$	Liu isotherm model	335.8	[46]
Bamboo	$AlCl_3$ activating agent	—	13.36	[69]
Magnetic mesoporous carbon composite	Hydrothermal carbonisation	Langmuir model	—	[70]
Smoked cigarette filters	KOH activation	Langmuir model	—	[71]
Sugarcane bagasse	Hydrothermal carbonization	Langmuir model	107.54	This study

spherical shaped holding an aromatic graphitic ring in cluster form holding hydroxyl and carboxyl groups. Such spherical carbon has the capacity to hold incoming pollutants or get functionalized with metals, improved functionality thereby promoting improved eradication of toxic pollutants [3].

3.8.4. Regeneration Studies. The efficiency of fabricated ACS was checked in removing CPF from water by assessing regeneration and reusability of as-synthesised adsorbent. This was performed by after removing CPF from water, ACS was separated and washed continuously with water and ethanol. The washed adsorbent was dried at 80°C for a certain period of time after which it was used for adsorption and desorption experiment. The experiment was repeatedly performed for 3 to 4 times for checking its capacity in removing the pollutant. Figure S3 shows the adsorption capacity of ACS after every wash with water and ethanol. It could be seen that after 4 times of washing reused ACS with ethanol, adsorption capacity retained to 71 mg g^{-1}. The main purpose of reusing the adsorbent is to reduce the cost involved in synthesis and testing process.

4. Use of Hydrothermally Derived Activated Spherical Carbons in Removing Toxic Pollutants

The activated spherical carbon derived from hydrothermal carbonisation of waste biomass or saccharide derivatives could be applied as adsorbents in removing toxic contaminants from water. Such carbons could be economically fabricated as it involves less energy consumption. To illustrate, activated carbon sphere derived from sucrose showed good adsorption capacity of 808.7 mg g-1 in removing sulfamethoxazole from water [12, 13]. Similarly, carbon derived from Agave Americana fibre and tannin showed good performance in removing tetracycline from water that showed faster equilibrium time with the help of macro- and mesopores in carbon surface [60]. Implementation of textile waste as carbon precursor yielded carbon hydrothermally that removed oxytetracycline from water with the capacity of 621.2 mg g^{-1} and 482.8 mg g^{-1} [61]. For promoting activity of carbon, hybrid sorbents had been introduced which showed improved activity due to synergetic effect induced by multiple interactions of hybrid sorbents. To illustrate, zero valent iron activated carbon was fabricated that was effectively applied in removing tetracycline antibiotics from water [62, 63]. Incorporation of hybrid nanoparticles with hydrothermal products could be encouraged for removing pharmaceutical compounds from water [64]. On comparing with all the above studies, it could pave the way that hydrothermally activated carbon spheres could be applied in the field of water research for eradicating waste pollutants with the view of preserving water resource for sustainable future.

5. Sustainable Development of CS/ACS as an Effective Adsorbent

HTC is a novel technology applied in converting biomass at wet condition to high fraction of carbon residue. There are various factors that govern effective generation of CS through HTC, namely, carbonization temperature, residence time, pH condition, and biomass nature/composition. The obtained carbonaceous product was exploited for removal of waste organic and inorganic pollutants from aqueous solution through various technologies like adsorption, flotation, catalytic degradation, and photolysis thereby promoting way for environmental remediation. Production of carbonaceous product from HTC could be modified using various methods of synthesis with or without catalyst. But all these effectiveness could be applied considering the production cost and economic feasibility. Development of carbonaceous product from HTC involves a lot of analogy in determining the multiple expenses like operating cost, maintenance, labour cost, and biomass acquirement and other expenses like distribution, transportation, electricity consumption, and production cost. Today, in order to reduce the cost of production, industries are demanding low budget biomass especially those that are coming from agricultural waste. To illustrate raw olive pomace after HTC, treatment

Table 4: Cost estimation.

Parameters	Approximate consumption	Cost ($)
0.1 M KOH	100 mL	1.76
Tubular furnace (700°C/2 hours)	10 kWh^{-1}	1.5
Nitrogen as inert gas atmosphere (30 mL/min)	1.02 kWh^{-1}	0.15
Sugarcane bagasse	250 g	Free of cost
Stainless steel HTC operation in muffle furnace (190°C for 18–20 hours)	2 kWh^{-1} Hence for maximum 20 hours of run = 40 kWh^{-1}	6.0
HTC reactor (190°C for 2 hours)	2 kWh^{-1} Hence for 2 hours = 4 kWh^{-1}	0.6
Total with HTC reactor		= 9.41 *US$*/500 g
Total without stainless steel HTC		= 4.01 *US$*/500 g

Note: the material was fabricated during the period of January–March 2021.

may yield 50% dry carbonaceous product whose production cost is estimated to be US$450. This seemed to improve the profitability ratio as raw biomass itself costs US$60/ton. Additionally, by reducing the electricity consumption charges, alternative approaches had been made like the application of renewable energy resources like solar power and wind energy which are being encouraged [2]. One of the promising applications of carbonaceous product is its application as energy storage material. This favours by reducing the fuel consumption in transportation units, add-on electricity at remote locations by integrating into energy grids [65]. It is considered as an effective approach because of its following advantages like being environmentally friendly, versatile, enhanced reaction rate, economic cost, and useful by-product production. Hence, it could be considered as an alternative source for regrowing resources like fuels by generating high end carbon materials. HTC process yields carbon materials that are highly resistant to decomposition. This process releases $1/3^{rd}$ of combustion energy in dehydration reaction even though they are considered as energy economic. This technology avoids predrying of biomass residue as the reaction occurs at wet condition. As carbon developed from HTC process is structurally enriched with oxygenated functional groups like polar groups on its surface, they could be adopted as effective adsorbent in removing desired pollutants from water, CO_2 capture from atmosphere, and many more [66]. To illustrate effective removal of SMX was achieved using porous carbon development from carbohydrate source using HTC technology. Developed carbon was estimated to be 1.6 MB/g based on reagents and production cost if the cost on labour and energy is controlled using alternatives [12, 13]. Hence, it could be suggested that carbonaceous products evolving from HTC process could be treated as an effective alternative approach for fabricating activated carbon at high production scale. Additionally functionalizing with surfactants, metal oxides or polymers may still have a chance of increasing its environmental applicability by removing the target pollutants.

5.1. Cost Estimation in Fabricating CS/ACS. Cost analysis helps in better understanding the sustainable fabrication of target material. To estimate the cost for developing CS/ACS for environmental pollutants remediation, equations could be considered that take the cost of energy consumption and reagents used in fabrication in estimation which is shown in Table 4. From the estimation, it could be seen that amount required for developing carbonaceous product from sugarcane bagasse from HTC is 18.82 *US$* per kg of sugarcane bagasse for stainless steel HTC. On the other hand for HTC reactor, it is 8.02 *US$* per kg of biomass [11].

6. Summary and Conclusion

Agricultural crop residues could be employed as a constructive carbonaceous product through the HTC process which finds its application in removing pollutants from water and in other fields. Sugarcane bagasse was converted into carbon using HTC followed by activation in inert gas atmosphere with alkali impregnation technique. As the development of porosity and surface area is less in the HTC process, material was allowed for activation at high temperature. Various characterizations were performed for understanding its chemical, physical, thermal science, surface area, and surface morphology. The formed material from HTC shows spherical structure with inner core carrying hydrophobic functional followed by hydrophilic functional groups on its outer ring with minimal number of pores carrying less surface area. These functional groups and enhanced pores are responsible for holding the target pollutant based on surface/chemical adsorption. After activation, using KOH, though the intensity of functional groups reduced, induced rough surface on ACS that additionally favoured removal of CPF from water. Batch adsorption studies revealed that mechanism of removal of CPF from water followed pseudo-second-order kinetics with multilayer heterogonous mode (Freundlich). The maximum adsorption capacity of ACS was estimated to be 110.008 $mg\,g^{-1}$. It could be suggested that the use of the HTC process is highly reliable,

feasible, economic, and sustainable due to its major advantages like less amount of energy consumption, versatility, use of wet biomass, and improved yield by-product.

Abbreviations

HTC: Hydrothermal carbonization
CPF: Ciprofloxacin hydrochloride
CS: Carbon sphere
ACS: Activated carbon spheres
PM: Particulate matter
SPM: Suspended particulate matter.

Data Availability

Data are available on request.

Conflicts of Interest

The author(s) declare(s) that they have no conflicts of interest.

Acknowledgments

This research work was sponsored and reinforced by the Institution of Engineers (India) (IEI, Kolkatta) under IEI R&D Grant-in-aid Scheme (Project ID: DR2020010; Reference No: R.6/2/DR/2019-20/RDDR2019010).

Supplementary Materials

Table S1: different mathematical models used in this work to fit the experimental data. Table S2: elemental composition of CS and ACS-K. Table S3: EDAX analysis of CS and ACS-K. Table S4: BET analysis. Figure S1: particle size distribution of CS and ACS. (a) Denotes particle size of CS and (b) ACS-KOH. Figure S2: TGA analysis for CS and ACS. (a) TGA of CS and (b) TGA of ACS-KOH. Figure S3: species distribution of CPF. Figure S4: regeneration of ACS using water and ethanol. *(Supplementary Materials)*

References

[1] S. Liu, X. Wang, H. Zhao, and W. Cai, "Micro/nano-scaled carbon spheres based on hydrothermal carbonization of agarose," *Colloids and Surfaces A: Physicochemical and Engineering Aspects*, vol. 484, pp. 386–393, 2015.

[2] A. Azzaz, B. Khiari, S. Jellali, C. M. Ghimbeu, and M. Jeguirim, "Hydrochars production, characterization and application for wastewater treatment: A review," *Renewable and Sustainable Energy Reviews*, vol. 127, article 109882, 2020.

[3] G. Prasannamedha and P. S. Kumar, "A review on contamination and removal of sulfamethoxazole from aqueous solution using cleaner techniques: present and future perspective," *Journal of Cleaner Production*, vol. 250, article 119553, 2020.

[4] M. Inada, N. Enomoto, J. Hojo, and K. Hayashi, "Structural analysis and capacitive properties of carbon spheres prepared by hydrothermal carbonization," *Advanced Powder Technology*, vol. 28, no. 3, pp. 884–889, 2017.

[5] T. Khan, A. S. Saud, S. S. Jamari, M. H. A. Rahim, J. W. Park, and H. J. Kim, "Hydrothermal carbonization of lignocellulosic biomass for carbon rich material preparation: a review," *Biomass and Bioenergy*, vol. 130, article 105384, 2019.

[6] M. Heidari, A. Dutta, B. Acharya, and S. Mahmud, "A review of the current knowledge and challenges of hydrothermal carbonization for biomass conversion," *Journal of the Energy Institute*, vol. 92, pp. 1779–1799, 2018.

[7] R. Li, L. Wang, and A. Shahbazi, "A review of hydrothermal carbonization of carbohydrates for carbon spheres preparation," *Trends in Renewable Energy*, vol. 1, no. 1, pp. 43–56, 2015.

[8] A. Deshmukh, S. D. Mhlanga, and N. J. Coville, "Carbon spheres," *Materials Science and Engineering*, vol. 70, no. 1-2, pp. 1–28, 2010.

[9] D. Congsomjit and C. Areeprasert, "Hydrochar-derived activated carbon from sugar cane bagasse employing hydrothermal carbonization and steam activation for syrup decolorization," *Biomass Conversion and Biorefinery*, vol. 11, no. 6, pp. 2569–2584, 2020.

[10] A. J. Romero-Anaya, M. Ouzzine, M. A. Lillo-Ródenas, and A. Linares-Solano, "Spherical carbons: synthesis, characterization and activation processes," *Carbon*, vol. 68, pp. 296–307, 2014.

[11] M. Zbair, H. Ait Ahsaine, and Z. Anfar, "Porous carbon by microwave assisted pyrolysis: an effective and low-cost adsorbent for sulfamethoxazole adsorption and optimization using response surface methodology," *Journal of Cleaner Production*, vol. 202, pp. 571–581, 2018.

[12] Y. Shi, G. Liu, L. Wang, and H. Zhang, "Activated carbons derived from hydrothermal impregnation of sucrose with phosphoric acid: remarkable adsorbents for sulfamethoxazole removal," *RSC Advances*, vol. 9, no. 31, pp. 17841–17851, 2019.

[13] Y. Shi, G. Liu, L. Wang, and H. Zhang, "Heteroatom-doped porous carbons from sucrose and phytic acid for adsorptive desulfurization and sulfamethoxazole removal: a comparison between aqueous and non-aqueous adsorption," *Journal of Colloid and Interface Science*, vol. 557, pp. 336–348, 2019.

[14] F.-C. Huang, C. K. Lee, Y. L. Han, W. C. Chao, and H. P. Chao, "Preparation of activated carbon using micro-nano carbon spheres through chemical activation," *Journal of the Taiwan Institute of Chemical Engineers*, vol. 45, no. 5, pp. 2805–2812, 2014.

[15] A. Jain, R. Balasubramanian, and M. P. Srinivasan, "Hydrothermal conversion of biomass waste to activated carbon with high porosity: a review," *Chemical Engineering Journal*, vol. 283, pp. 789–805, 2016.

[16] M. J. Sukhesh and P. V. Rao, "Anaerobic digestion of crop residues: technological developments and environmental impact in the Indian context," *Biocatalysis and Agricultural Biotechnology*, vol. 16, pp. 513–528, 2018.

[17] M. T. Reza, J. Mumme, and A. Ebert, "Characterization of hydrochar obtained from hydrothermal carbonization of wheat straw digestate," *Biomass Conversion and Biorefinery*, vol. 5, no. 4, pp. 425–435, 2015.

[18] M. Zhao, B. Li, J. X. Cai, C. Liu, K. G. McAdam, and K. Zhang, "Thermal & chemical analyses of hydrothermally derived carbon materials from corn starch," *Fuel Processing Technology*, vol. 153, pp. 43–49, 2016.

[19] R. Khoshbouy, F. Takahashi, and K. Yoshikawa, "Preparation of high surface area sludge-based activated hydrochar via hydrothermal carbonization and application in the removal

of basic dye," *Environmental Research*, vol. 175, pp. 457–467, 2019.

[20] C. A. Melo, F. H. S. Junior, M. C. Bisinoti, A. B. Moreira, and O. P. Ferreira, "Transforming sugarcane bagasse and vinasse wastes into hydrochar in the presence of phosphoric acid: an evaluation of nutrient contents and structural properties," *Waste and Biomass Valorization*, vol. 8, no. 4, pp. 1139–1151, 2017.

[21] S. Feshki, "Synthesis of carbon spheres of controlled size by hydrothermal method," *Journal of Nanostructures*, vol. 4, pp. 295–301, 2014.

[22] F. Veltri, F. Alessandro, A. Scarcello et al., "Porous carbon materials obtained by the hydrothermal carbonization of orange juice," *Nanomaterials*, vol. 10, no. 4, p. 655, 2020.

[23] L. Muniandy, F. Adam, A. R. Mohamed, and E. P. Ng, "The synthesis and characterization of high purity mixed microporous/mesoporous activated carbon from rice husk using chemical activation with NaOH and KOH," *Microporous and Mesoporous Materials*, vol. 197, pp. 316–323, 2014.

[24] P. Sun, K. Zhang, S. Shang, J. Song, and D. Wang, "Sustainable production of activated carbon spheres from ethyl cellulose," *RSC Advances*, vol. 6, no. 98, pp. 95656–95662, 2016.

[25] S. Liu, J. Sun, and Z. Huang, "Carbon spheres/activated carbon composite materials with high Cr(VI) adsorption capacity prepared by a hydrothermal method," *Journal of Hazardous Materials*, vol. 173, no. 1-3, pp. 377–383, 2010.

[26] Z. Liu, F. S. Zhang, and J. Wu, "Characterization and application of chars produced from pinewood pyrolysis and hydrothermal treatment," *Fuel*, vol. 89, no. 2, pp. 510–514, 2010.

[27] Y. Mi, W. Hu, Y. Dan, and Y. Liu, "Synthesis of carbon microspheres by a glucose hydrothermal method," *Materials Letters*, vol. 62, no. 8-9, pp. 1194–1196, 2008.

[28] G. Prasannamedha, P. S. Kumar, R. Mehala, T. J. Sharumitha, and D. Surendhar, "Enhanced adsorptive removal of sulfamethoxazole from water using biochar derived from hydrothermal carbonization of sugarcane bagasse," *Journal of Hazardous Materials*, vol. 407, article 124825, 2021.

[29] Z. Liu and F. S. Zhang, "Removal of copper (II) and phenol from aqueous solution using porous carbons derived from hydrothermal chars," *Desalination*, vol. 267, no. 1, pp. 101–106, 2011.

[30] G. Pari, S. Darmawan, and B. Prihandoko, "Porous carbon spheres from hydrothermal carbonization and KOH activation on cassava and tapioca flour raw material," *Procedia Environmental Sciences*, vol. 20, pp. 342–351, 2014.

[31] M. Li, W. Li, and S. Liu, "Hydrothermal synthesis, characterization, and KOH activation of carbon spheres from glucose," *Carbohydrate Research*, vol. 346, no. 8, pp. 999–1004, 2011.

[32] K. C. Bedin, A. C. Martins, A. L. Cazetta, O. Pezoti, and V. C. Almeida, "KOH-activated carbon prepared from sucrose spherical carbon: adsorption equilibrium, kinetic and thermodynamic studies for methylene blue removal," *Chemical Engineering Journal*, vol. 286, pp. 476–484, 2016.

[33] H. Hadoun, Z. Sadaoui, N. Souami, D. Sahel, and I. Toumert, "Characterization of mesoporous carbon prepared from date stems by H_3PO_4 chemical activation," *Applied Surface Science*, vol. 280, pp. 1–7, 2013.

[34] F. Liu, R. Yu, and M. Guo, "Hydrothermal carbonization of forestry residues: influence of reaction temperature on holocellulose-derived hydrochar properties," *Journal of Materials Science*, vol. 52, no. 3, pp. 1736–1746, 2016.

[35] M. Liang, J. Wang, M. Zhao et al., "Borax-assisted hydrothermal carbonization to fabricate monodisperse carbon spheres with high thermostability," *Materials Research Express*, vol. 6, no. 6, 2019.

[36] K. C. Bedin, A. L. Cazetta, I. P. A. F. Souza et al., "Porosity enhancement of spherical activated carbon: influence and optimization of hydrothermal synthesis conditions using response surface methodology," *Journal of Environmental Chemical Engineering*, vol. 6, no. 1, pp. 991–999, 2018.

[37] L. Zhao, Z. Bacsik, N. Hedin et al., "Carbon dioxide capture on amine-rich carbonaceous materials derived from glucose," *ChemSusChem*, vol. 3, no. 7, pp. 840–845, 2010.

[38] M. Naderi and M. Vesali-Naseh, "Hydrochar-derived fuels from waste walnut shell through hydrothermal carbonization: characterization and effect of processing parameters," *Biomass Conversion and Biorefinery*, vol. 11, no. 5, pp. 1443–1451, 2019.

[39] Z. Liu and F. S. Zhang, "Removal of lead from water using biochars prepared from hydrothermal liquefaction of biomass," *Journal of Hazardous Materials*, vol. 167, no. 1-3, pp. 933–939, 2009.

[40] S. K. R. Patil, J. Heltzel, and C. R. F. Lund, "Comparison of structural features of humins formed catalytically from glucose, fructose, and 5-hydroxymethylfurfuraldehyde," *Energy & Fuels*, vol. 26, no. 8, pp. 5281–5293, 2012.

[41] T. Wang, X. Liu, C. Ma et al., "A two step hydrothermal process to prepare carbon spheres from bamboo for construction of core–shell non-metallic photocatalysts," *New Journal of Chemistry*, vol. 42, no. 8, pp. 6515–6524, 2018.

[42] M. Sevilla and A. . B. Fuertes, "Chemical and structural properties of carbonaceous products obtained by hydrothermal carbonization of saccharides," *Chemistry - A European Journal*, vol. 15, no. 16, pp. 4195–4203, 2009.

[43] H. Cai, X. Lin, L. Tian, and X. Luo, "One-step hydrothermal synthesis of carbonaceous spheres from glucose with an aluminum chloride catalyst and its adsorption characteristic for uranium(VI)," *Industrial & Engineering Chemistry Research*, vol. 55, no. 36, pp. 9648–9656, 2016.

[44] N. Sharifpour, F. M. Moghaddam, G. Mardani, and M. Malakootian, "Evaluation of the activated carbon coated with multiwalled carbon nanotubes in removal of ciprofloxacin from aqueous solutions," *Applied Water Science*, vol. 10, no. 6, p. 140, 2020.

[45] T. J. al-Musawi, A. H. Mahvi, A. D. Khatibi, and D. Balarak, "Effective adsorption of ciprofloxacin antibiotic using powdered activated carbon magnetized by iron(III) oxide magnetic nanoparticles," *Journal of Porous Materials*, vol. 28, no. 3, pp. 835–852, 2021.

[46] C. de Oliveira Carvalho, D. L. Costa Rodrigues, É. C. Lima, C. Santanna Umpierres, D. F. Caicedo Chaguezac, and F. Machado Machado, "Kinetic, equilibrium, and thermodynamic studies on the adsorption of ciprofloxacin by activated carbon produced from Jerivá (Syagrus romanzoffiana)," *Environmental Science and Pollution Research*, vol. 26, no. 5, pp. 4690–4702, 2018.

[47] M. E. Mahmoud, S. R. Saad, A. M. El-Ghanam, and R. H. A. Mohamed, "Developed magnetic Fe_3O_4–MoO_3-AC nanocomposite for effective removal of ciprofloxacin from water," *Materials Chemistry and Physics*, vol. 257, article 123454, 2020.

[48] A. Chandrasekaran, C. Patra, S. Narayanasamy, and S. Subbiah, "Adsorptive removal of Ciprofloxacin and Amoxicillin from single and binary aqueous systems using acid-

activated carbon from *Prosopis juliflora*," *Environmental Research*, vol. 188, article 109825, 2020.

[49] S. Lagergren, "About the theory of so-called adsorption of soluble substances, Kungliga Svenska Vetenskapsakademiens," *Handlingar*, vol. 24, no. 4, pp. 1–39, 1898.

[50] Y. S. Ho and G. McKay, "Pseudo-second order model for sorption processes," *Process Biochemistry*, vol. 34, no. 5, pp. 451–465, 1999.

[51] W. J. Weber and J. C. Morris, "Kinetics of adsorption on carbon from solution," *Journal Sanitary Engineering Division Proceedings, American Society of Civil Engineers*, vol. 89, no. 2, pp. 31–59, 1963.

[52] Y. X. Wang, H. H. Ngo, and W. S. Guo, "Preparation of a specific bamboo based activated carbon and its application for ciprofloxacin removal," *Science of the Total Environment*, vol. 533, pp. 32–39, 2015.

[53] Y. Wang, R. Yang, M. Li, and Z. Zhao, "Hydrothermal preparation of highly porous carbon spheres from hemp (*Cannabis sativa* L.) stem hemicellulose for use in energy-related applications," *Industrial Crops and Products*, vol. 65, pp. 216–226, 2015.

[54] M. E. Peñafiel, J. M. Matesanz, E. Vanegas, D. Bermejo, R. Mosteo, and M. P. Ormad, "Comparative adsorption of ciprofloxacin on sugarcane bagasse from Ecuador and on commercial powdered activated carbon," *Science of the Total Environment*, vol. 750, article 141498, 2020.

[55] I. Langmuir, "The adsorption of gases on plane surfaces of glass, mica and platinum," *Journal of the American Chemical Society*, vol. 40, no. 9, pp. 1361–1403, 1918.

[56] H. M. F. Freundlich, "Über die adsorption in Lösungen," *Journal of Physical Chemistry*, vol. 57U, no. 1, pp. 385–470, 1906.

[57] M. Temkin and V. Pyzhev, "Kinetics of ammonia synthesis on promoted iron catalysts," *Acta Physicochimica URSS*, vol. 12, pp. 217–222, 1940.

[58] M. Wang, G. Li, L. Huang et al., "Study of ciprofloxacin adsorption and regeneration of activated carbon prepared from *Enteromorpha prolifera* impregnated with H_3PO_4 and sodium benzenesulfonate," *Ecotoxicology and Environmental Safety*, vol. 139, pp. 36–42, 2017.

[59] M. Malakootian, A. Nasiri, and H. Mahdizadeh, "Preparation of $CoFe_2O_4$/activated carbon@chitosan as a new magnetic nanobiocomposite for adsorption of ciprofloxacin in aqueous solutions," *Water Science and Technology*, vol. 78, no. 10, pp. 2158–2170, 2018.

[60] T. Selmi, A. Sanchez-Sanchez, P. Gadonneix et al., "Tetracycline removal with activated carbons produced by hydrothermal carbonisation of Agave Americana fibres and mimosa tannin," *Industrial Crops and Products*, vol. 115, pp. 146–157, 2018.

[61] G. Duman, "Preparation of novel porous carbon from hydrothermal pretreated textile wastes: effects of textile type and activation agent on structural and adsorptive properties," *Journal of Water Process Engineering*, vol. 43, article 102286, 2021.

[62] K. A. Azalok, A. A. Oladipo, and M. Gazi, "Hybrid MnFe-LDO-biochar nanopowders for degradation of metronidazole *via* UV- light-driven photocatalysis: Characterization and mechanism studies," *Chemosphere*, vol. 268, article 128844, 2021.

[63] Y.-X. Song, S. Chen, N. You, H. T. Fan, and L. N. Sun, "Nanocomposites of zero-valent iron@Activated carbon derived from corn stalk for adsorptive removal of tetracycline antibiotics," *Chemosphere*, vol. 255, article 126917, 2020.

[64] K. A. Azalok, A. A. Oladipo, and M. Gazi, "UV-light-induced photocatalytic performance of reusable MnFe-LDO-biochar for tetracycline removal in water," *Journal of Photochemistry and Photobiology A: Chemistry*, vol. 405, article 112976, 2021.

[65] M.-M. Titirici and M. Antonietti, "Chemistry and materials options of sustainable carbon materials made by hydrothermal carbonization," *Chemical Society Reviews*, vol. 39, no. 1, pp. 103–116, 2010.

[66] B. Hu, K. Wang, L. Wu, S. H. Yu, M. Antonietti, and M. M. Titirici, "Engineering carbon materials from the hydrothermal carbonization process of biomass," *Advanced Materials*, vol. 22, no. 7, pp. 813–828, 2010.

[67] B. Zhang, X. Han, P. Gu, S. Fang, and J. Bai, "Response surface methodology approach for optimization of ciprofloxacin adsorption using activated carbon derived from the residue of desilicated rice husk," *Journal of Molecular Liquids*, vol. 238, pp. 316–325, 2017.

[68] X. Zhu, D. C. W. Tsang, F. Chen, S. Li, and X. Yang, "Ciprofloxacin adsorption on graphene and granular activated carbon: kinetics, isotherms, and effects of solution chemistry," *Environmental Technology*, vol. 36, no. 24, pp. 3094–3102, 2015.

[69] A. Guellati, R. Maachi, T. Chaabane, A. Darchen, and M. Danish, "Aluminum dispersed bamboo activated carbon production for effective removal of ciprofloxacin hydrochloride antibiotics: optimization and mechanism study," *Journal of Environmental Management*, vol. 301, article 113765, 2022.

[70] S. Shi, Y. Fan, and Y. Huang, "Facile low temperature hydrothermal synthesis of magnetic mesoporous carbon nanocomposite for adsorption removal of ciprofloxacin antibiotics," *Industrial and Engineering Chemistry Research*, vol. 52, no. 7, pp. 2604–2612, 2013.

[71] X. Zhang, J. Xu, Z. Lv et al., "Preparation and utilization of cigarette filters based activated carbon for removal CIP and SDS from aqueous solutions," *Chemical Physics Letters*, vol. 747, article 137343, 2020.